One-pot peptide cyclisation and surface modification of photosensitiser-loaded red blood cells for targeted photodynamic therapy

Received 00th January 20xx,
Accepted 00th January 20xx

DOI: 10.1039/x0xx00000x

Jacky C. H. Chu,[a] Chihao Shao,[b] Summer Y. Y. Ha,[a] Wing-Ping Fong,[c] Clarence T. T. Wong*[b] and Dennis K. P. Ng*[a]

We report herein a one-pot approach to cyclise a tumour-targeting peptide and conjugate it on the surface of red blood cells loaded with a boron dipyrromethene-based photosensitiser using a bifunctional linker consisted of a bis(bromomethyl)phenyl and an *ortho*-phthalaldehyde units. This cell-based photosensitiser with surface modification with cyclic RGD peptide moieties can selectively bind against the $\alpha_v\beta_3$ integrin-overexpressed cancer cells, leading to enhanced photocytotoxicity. The results demonstrate that this facile strategy is effective for live-cell surface modification for a wide range of applications.

Cell membrane is a complex interface composed of multiple functional molecules, including proteins, lipids and carbohydrates. It plays an important role in regulating selective transport of molecules, inter-cellular communications, as well as interactions with the environment.[1] The understanding and manipulation of cell membrane are crucial for the studies of cellular behaviour and the translational research on innovative biotechnological applications and therapeutics development.[2,3] Cell membrane conjugation has been performed on mammalian cells and bacterial cell envelope.[4-6] In general, there are three approaches to engineer the cell surface, namely genetic modification, enzymatic ligation and chemical/physical bioconjugation. In particular, modification of cell surface by chemical strategies may enable a range of cell-surface functionalisation, such as tailoring the ligand presentation and the spatiotemporal control of the cell-cell interactions.[7,8] Exogenous cargos, including peptides, proteins, DNA, polymers and nanoparticles have been chemically conjugated onto the cell membranes.[9-13] The primary amino groups on the native cell surface proteins have been the target for conjugation using a range of coupling reagents, such as *N*-hydroxysuccinimide (NHS) esters and cyanuric chloride, or *via* ester aldehyde azaelectrocyclisation.[5] These chemical reactions, however, have the drawbacks of relatively low coupling efficiency, low specificity and generation of side products. Moreover, the reactants in these chemical reactions are usually unstable in neutral pH aqueous buffer. Ideally, the reactions on the fragile living cells should be rapid to minimise diffusion of the reactants into the cellular compartments and production of side products. The reactants should also be stable in physiological conditions and non-cytotoxic. To meet these demands, there has been considerable interest in the development of advanced methodologies for specific cell membrane modification.

Recently, the phthalaldehyde-amine capture (PAC) reaction has emerged as a promising amine-specific bioconjugation strategy. It uses the *ortho*-phthalaldehyde (OPA) moiety to effectively form covalent bonds with amine-containing compounds under physiological conditions.[14,15] The PAC reaction is faster and more specific than the NHS-ester amide formation. The OPA precursor is highly stable in the absence of amine. Recently, we have utilised this strategy to efficiently conjugate a phthalocyanine-based photosensitiser to different biomolecules, nanoparticles and glass surface for photodynamic treatment against cancers and bacteria.[16] We report herein an extension of this study, using this reaction for cell surface modification.

To visualise the cell surface conjugation mediated by the PAC reaction, an OPA-functionalised methylene blue (**MB-OPA**) was synthesised for labelling. As shown in the synthetic scheme (Fig. 1A), reduction of the previously reported methyl ester acetal-protected OPA **1**[14] with $LiAlH_4$ gave the hydroxyl analogue **2**, which was then transformed into tosylate **3**. Nucleophilic substitution with CH_3NH_2, followed by the reaction with methylene blue (**4**) and acidic treatment with trifluoroacetic acid (TFA) led to the formation of **MB-OPA**. The cell surface labelling experiment was performed by using AsPC-1 human pancreatic adenocarcinoma cells as a model cell line (Fig. 1B). The cells were incubated with 2 μM of **MB-OPA** in phosphate-buffered saline (PBS) for 15 min at 37 °C, and then examined using confocal fluorescence microscopy. Fluorescence could clearly be observed on the cell surface, demonstrating that **MB-OPA** had been conjugated efficiently on

[a] *Department of Chemistry, The Chinese University of Hong Kong, Shatin, N.T., Hong Kong, China. E-mail: dkpn@cuhk.edu.hk*
[b] *Department of Applied Biology and Chemical Technology, The Hong Kong Polytechnic University, Kowloon, Hong Kong, China. E-mail: clarence-tt.wong@polyu.edu.hk*
[c] *School of Life Sciences, The Chinese University of Hong Kong, Shatin, N.T., Hong Kong, China*
†Electronic Supplementary Information (ESI) available. See DOI: 10.1039/x0xx00000x

the living cell surface (Fig. 1C). Without the OPA moiety, **4** was not able to stain the cell surface.

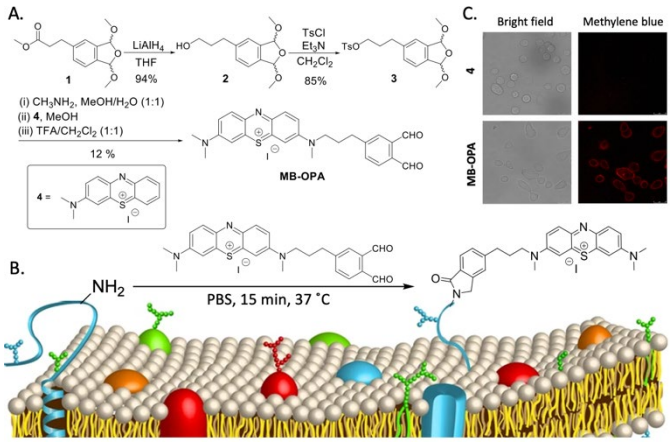

Fig. 1 (A) Synthetic scheme for **MB-OPA**. (B) Schematic diagram of conjugating **MB-OPA** on the cell membrane. (C) Bright-field and fluorescence images of AsPC-1 cells after incubation with **4** or **MB-OPA** (both at 2 μM) for 15 min.

After demonstrating the successful cell surface modification with **MB-OPA**, we further extended this methodology to conjugate tumour-targeting cyclic peptide moieties on the surface of photosensitiser-loaded red blood cells (RBCs) that can serve as cell-based photosensitisers for targeted photodynamic therapy (PDT). PDT has emerged as a promising anti-cancer treatment modality.[17,18] It utilises a photosensitiser, light and oxygen to generate cytotoxic reactive oxygen species (ROS) upon photosensitisation. The treatment involves a straightforward and non-invasive procedure that requires only a single drug injection followed by localised light irradiation, and can be performed on an outpatient basis. Although PDT has been approved to treat a number of superficial and localised cancers, it is still hampered by the limited target specificity of photosensitisers, which causes undesired phototoxicity and affects the effective dose.[19-21] Furthermore, most of the photosensitisers are generally insoluble in the aqueous physiological environment due to their hydrophobic extended π-system. Accumulative evidence has shown that using RBCs as a carrier of photosensitisers can improve the PDT efficacy by increasing the oxygen content and reduce the undesired phototoxicity.[22,23] In fact, RBCs are promising drug carriers because of their high loading capacity, biocompatibility, large membrane area for modification and high elasticity to enter the leaky capillaries in tumour.[24-26] The lack of facile methods of cell surface modification, however, has hindered the further development.

Recently, we have reported a facile one-pot procedure for *in situ* peptide cyclisation and photosensitiser conjugation for targeted PDT. This methodology utilises a bifunctional linker containing a bis(bromomethyl)phenyl moiety and an azide or cyclopentadiene unit for facilitating the nucleophilic substitution with two cysteine residues of the linear peptides and the cycloaddition with functionalised photosensitisers respectively.[27-29] Based on this strategy, we have designed a bifunctional linker that contains a bis(bromomethyl)phenyl moiety and an OPA unit. Whilst the former can promote peptide cyclisation, the latter can facilitate the surface modification of RBCs *via* PAC coupling as demonstrated above. These two processes can proceed *in situ* through a one-pot procedure.

This linker (compound **5**) was prepared by nucleophilic mono-substitution of 1,3,5-tris(bromomethyl)benzene with **2** in the presence of NaH (Fig. 2A). For the peptide, an $\alpha_v\beta_3$ integrin-targeting RGD peptide containing two cysteine residues at the termini (AcNH-CRGDfC-$CONH_2$) was selected and prepared manually using the standard 9-fluorenylmethoxycarbonyl solid-phase peptide synthesis protocol. The use of cyclic peptides not only can enhance the target specificity and binding affinity, but also increase the stability in serum compared to the linear counterparts.[30,31] The linker **5** was first treated with TFA in water (1:1 v/v) to remove the acetal protecting group, and then coupled with the linear RGD peptide sequence *via* site-selective dibenzylation with the two cysteine residues in borate buffer (pH 8.5, 1 mM). Analytical reverse-phase HPLC was used to monitor the cyclisation process. After 2 h, the conversion was found to be 91% and the target conjugate **cRGD-OPA** was isolated in 71% (Fig. 2B). Without further purification, **cRGD-OPA** was conjugated onto rabbit RBCs in Hank's Balanced Salt Solution (HBSS) through the PAC reaction at room temperature for 30 min. After the reaction, the RBCs were washed by HBSS three times to give the cyclic RGD-conjugated RBCs (**cRGD-RBC**).

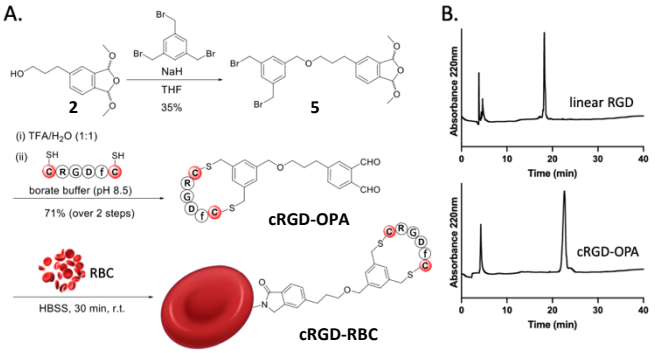

Fig. 2 (A) Synthetic scheme for **cRGD-OPA** and immobilisation on RBCs. (B) HPLC chromatograms of the linear RGD peptide and **cRGD-OPA**.

For the photosensitiser component, three different near-infrared photosensitisers were selected to be encapsulated inside the RBCs, namely zinc(II) phthalocyanine (ZnPc), distyryl boron dipyrromethene (BODIPY) with two triethylene glycol chains (**dsBDP(TEG)$_2$**) and the dicarboxyl analogue **dsBDP(COOH)$_2$** (Fig. 3A). The synthetic routes for the latter two compounds are given in Scheme S1 (ESI†). Their UV-Vis spectra in *N,N*-dimethylformamide (DMF) (Fig. S1, ESI†) were typical as those of other distyryl BODIPYs.[27] The strongest band at 660 (for **dsBDP(TEG)$_2$**) or 665 nm (for **dsBDP(COOH)$_2$**) strictly obeyed the Beer-Lambert law. Upon excitation at 610 nm, a strong fluorescence emission was observed at 691/700 nm with a fluorescence quantum yield (Φ_F) of 0.22/0.20 respectively relative to ZnPc (Φ_F = 0.28 in DMF) (Table S1, ESI†).[28] The shapes of these spectra were not changed significantly in PBS with Tween 80 (0.1% v/v) (Figs. S2 and S3, ESI†), showing that these two BODIPY derivatives remained essentially non-aggregated in

this aqueous medium. By using 1,3-diphenylisobenzofuran as the singlet oxygen scavenger,[32] their singlet oxygen quantum yields (Φ_Δ) were also determined to be 0.54/0.52 respectively relative to ZnPc (Φ_Δ = 0.56)[28] in DMF (Table S1, ESI†) and their efficiencies were also comparable in PBS with Tween 80 (0.1% v/v) (Fig. S4, ESI†).

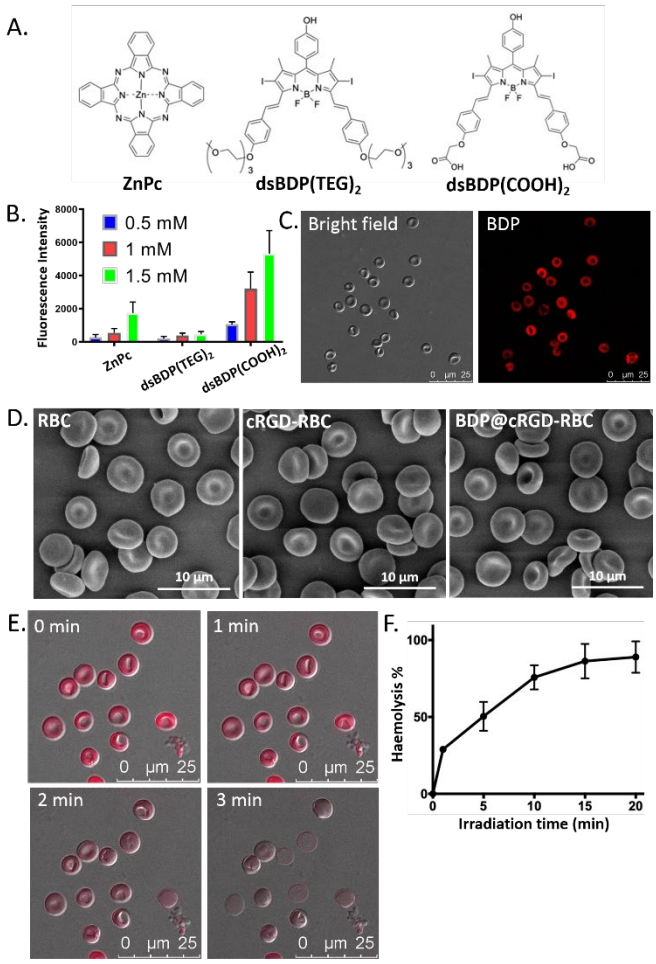

Fig. 3 (A) Molecular structures of the three photosensitisers loaded into RBCs. (B) The quantified fluorescence intensities of the RBCs encapsulated with different concentrations of the three photosensitisers as determined by flow cytometry. Data are expressed as the mean ± standard error of the mean (SEM) of three independent experiments. (C) Confocal images of **BDP@cRGD-RBC**. (D) Scanning electron microscopic images of the native RBCs, **cRGD-RBC** and **BDP@cRGD-RBC**. (E) Time-lapse confocal images of **BDP@cRGD-RBC** being irradiated by a 638-nm laser of the confocal microscope. (F) Haemolysis percentage of **BDP@cRGD-RBC** upon light irradiation (λ > 610 nm, 23 mW cm^{-2}, 28 J cm^{-2}). Data are expressed as the mean ± SEM of three independent experiments.

These photosensitisers were then loaded into RBCs *via* an osmotic shock technique according to the previously reported procedure.[33] The RBCs were first swollen in a hypotonic NaCl solution (0.65% w/v) at 4 °C for 5 min to loosen the membrane. After centrifugation, different concentrations of these photosensitisers were added to diffuse into the swollen RBCs at 4 °C for 10 min. Afterwards, a higher concentration of hypertonic NaCl solution (9% w/v) was used to seal the RBC membrane at room temperature over 30 min. The suspension was further washed with isotonic HBSS to afford the photosensitiser-loaded RBCs. The uptake of the dyes was examined using flow cytometry. As shown in Fig. 3B, the intracellular fluorescence intensity of the RBCs loaded with **dsBDP(COOH)$_2$** was significantly higher compared with that of the other two photosensitisers, showing that the nature and the substituents of the dyes played a crucial role. Therefore, this photosensitiser was chosen for the subsequent studies.

The loading of **dsBDP(COOH)$_2$** into the cyclic RGD-conjugated RBCs was then performed using the same method. The absorption spectrum of the resulting cell-based photosensitiser, labelled as **BDP@cRGD-RBC**, in PBS showed the typical absorption bands of haemoglobin and distyryl BODIPYs, spreading widely in the UV-Vis region (Fig. S5, ESI†), indicating the successful loading of the dye into the RBCs. The loading as determined by electronic absorption spectroscopy for the lysed cells was found to be *ca.* 1.9 nmol in 3 x 10^4 RBCs. The broadened and red-shifted band of **dsBDP(COOH)$_2$** at *ca.* 700 nm indicated that the dye was slightly aggregated inside the RBCs. Nevertheless, the system was still fluoresced (at 695 nm) in PBS upon excitation at 610 nm (Fig. S6, ESI†). Confocal microscopy also showed a strong red fluorescence image for the cells (Fig. 3C). All the modifications did not alter the native biconcave structure of RBCs as revealed by scanning electron microscopy (Fig. 3D). However, upon irradiation by the laser at 638 nm equipped in the confocal microscope, the cells showed gradual haemolysis over 3 min (Fig. 3E). The extent of haemolysis was also measured upon irradiation with light after passing through a colour glass filter with a cut-on wavelength at 610 nm (fluence rate = 23 mW cm^{-2}) (Fig. S7, ESI†). After 20 min, about 80% of the cells were disrupted likely by the ROS generated by the photosensitiser inside the RBC cavity (Fig. 3F).

The cellular binding of **BDP@cRGD-RBC** was then studied using a range of cancer cell lines with different expression levels of $\alpha_v\beta_3$ integrin, including the $\alpha_v\beta_3$-positive U87-MG human glioblastoma cells and A549 human lung carcinoma cells and the $\alpha_v\beta_3$-negative MCF-7 human breast adenocarcinoma cells and HEK-293 human embryonic kidney cells.[27,34] The non-cRGD-conjugated **BDP@RBC** was also studied for comparison. The cells were incubated with approximately 3 x 10^6 cells of **BDP@cRGD-RBC** or **BDP@RBC** for 30 min, and then examined using confocal microscopy. As shown in Fig. S8 (ESI†), strong fluorescence could be observed for **BDP@cRGD-RBC** in U87-MG and A549 cells, but not in MCF-7 and HEK-293 cells, while for **BDP@RBC**, the intracellular fluorescence remained very weak for all the four cell lines. To better visualise the binding, U87-MG and A549 cells were pre-stained with CellTracker Green. The high-magnification and Z-stack double-stained confocal images clearly showed that **BDP@cRGD-RBC** (in red) were attached to the U87-MG and A549 cells (in green) (Fig. 4). These results demonstrated that this novel one-pot reaction could efficiently modify the surface of RBCs and endow them with a tumour-targeting capability.

After demonstrating the selective binding ability of **BDP@cRGD-RBC**, we further investigated the light-induced release of photosensitiser molecules from the RBCs into A549 cells. After incubation with **BDP@cRGD-RBC** for 30 min, the unbound RBCs were washed away with PBS. Confocal images

were taken at different time points during light irradiation (λ > 610 nm, 23 mW cm^{-2}) (Fig. S9, ESI†). Before the light irradiation, the fluorescent RBCs were clearly attached to the A549 cells. After 3 min of irradiation, some of the RBCs were lysed and the photosensitiser was internalised into the A549 cells as shown by the shift of the fluorescence signal. Further increase of the light dose resulted in decrease in fluorescence intensity due to the photo-bleaching of the photosensitiser. After 20 min of light irradiation, nuclear condensation of the A549 cells was observed, which is an indication of cell death.[35]

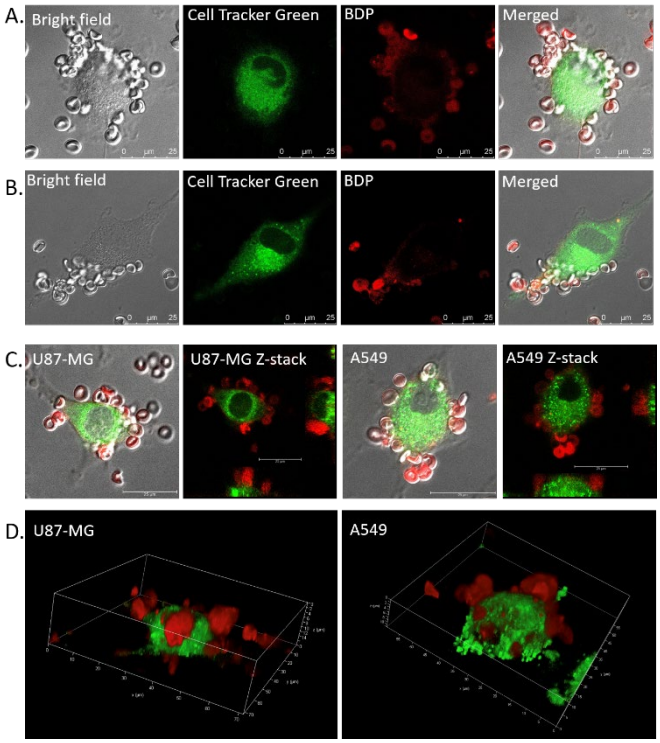

Fig. 4 The double staining confocal images of **BDP@cRGD-RBC** (in red) binding onto (A) U87-MG and (B) A549 cells (in green). (C) The Z-stack confocal images of the binding between **BDP@cRGD-RBC** and U87-MG or A549 cells. (D) The confocal 3D reconstruction images of **BDP@cRGD-RBC** and U87-MG or A549 cells.

The generation of ROS by **BDP@cRGD-RBC** inside these cancer cells was then studied using the common ROS probe 2′,7′-dichlorodihydrofluorescein diacetate (H_2DCFDA), which produces a highly fluorescent product, namely 2′,7′-dichlorofluorescein (DCF), upon oxidation by ROS.[36] As shown in Fig. 5, strong green fluorescence could only be observed in the $\alpha_v\beta_3$-positive U87-MG and A549 cells in the presence of light irradiation (λ > 610 nm, 23 mW cm^{-2}, 14 J cm^{-2}). For the $\alpha_v\beta_3$-negative MCF-7 and HEK-293 cells even upon irradiation and for the dark condition, all the four cell lines could not give noticeable fluorescence. For the non-cRGD-conjugated **BDP@RBC**, fluorescence could not be observed for all the four cell lines both in the absence and presence of light irradiation (Fig. S10, ESI†). To further examine whether the ROS generated can eradicate the cancer cells, live/dead double staining was also performed to identify the dead cells [stained in red with propidium iodide (PI)] and the viable cells (stained in green with Calcein AM). Upon incubation with **BDP@cRGD-RBC** followed by light irradiation for 10 min (λ > 610 nm, 23 mW cm^{-2}, 14 J cm^{-2}), there was a reduction in viable cells and an increase in the population of dead cells for U87-MG and A549 cells, but not for the other conditions (Fig. 6). As expected, no dead cells could be detected for **BDP@RBC** (Fig. S11, ESI†). These results further confirmed that **BDP@cRGD-RBC** could specifically bind to the $\alpha_v\beta_3$ integrin-overexpressed cancer cells and the photosensitiser molecules inside the RBC cavity could be released upon light irradiation, eventually eradicating the cancer cells by the ROS generated.

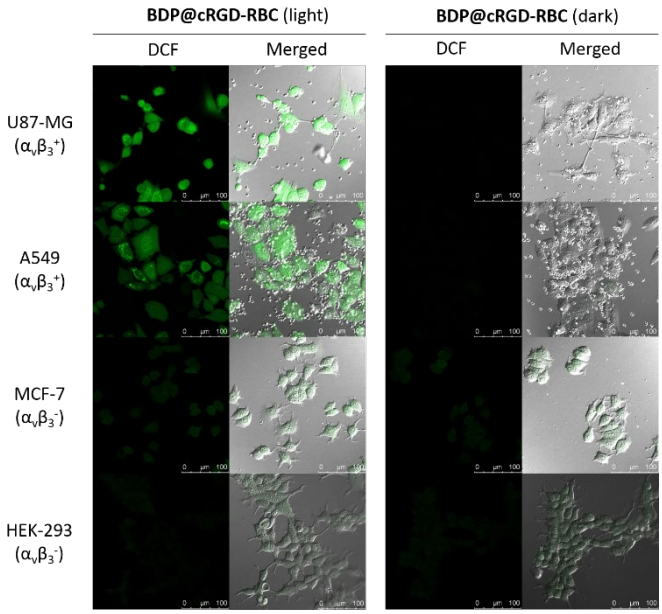

Fig. 5 Intracellular ROS production as reflected by the intracellular fluorescence of DCF in U87-MG, A549, MCF-7 and HEK-293 cells after incubation with **BDP@cRGD-RBC** for 30 min, followed by light irradiation for 10 min (λ > 610 nm, 23 mW cm^{-2}, 14 J cm^{-2}).

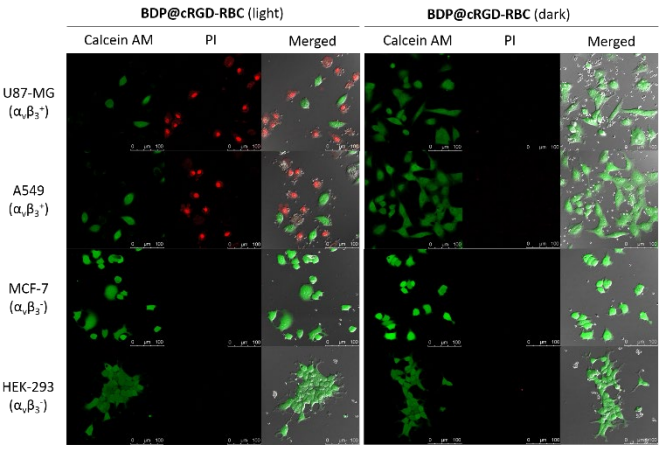

Fig. 6 Live/dead double staining of different cell lines upon treatment with **BDP@cRGD-RBC** with or without light irradiation for 10 min (λ > 610 nm, 23 mW cm^{-2}, 14 J cm^{-2}).

To quantify the cell viability, MTT [3-(4,5-dimethylthiazol-2-yl)-2,5-diphenyl-tetrazolium bromide] assay was performed for **BDP@cRGD-RBC** against U87-MG and MCF-7 cells (Fig. 7A). The results showed that without light irradiation, this cell-based

photosensitiser was not cytotoxic towards these two cell lines. However, upon light irradiation (λ > 610 nm, 23 mW cm^{-2}, 28 J cm^{-2}), it exhibited substantial cytotoxicity for the $\alpha_v\beta_3$-positive U87-MG cells with an IC_{50} value, which is defined as the amount of dye required to kill 50% of the cells, of 132 nmol in term of the amount of **dsBDP(COOH)$_2$**. For the $\alpha_v\beta_3$-negative MCF-7 cells, it remained non-cytotoxic. These results are consistent with those of the live/dead double staining experiment (Fig. 6).

To further investigate the cell death mechanism, U87-MG and MCF-7 cells were co-stained with annexin V-green fluorescent protein (GFP) and PI after being treated with **BDP@cRGD-RBC** or **BDP@RBC** as the control. The results are shown in Fig. S12 (ESI†) and summarised in Fig. 7B. It can be seen that a very low percentage of cell death (< 5%) was observed for both the cell lines after the treatment with **BDP@RBC** regardless of whether light irradiation was applied, which could be attributed to the negligible binding of **BDP@RBC** to these cells. In contrast, for the U87-MG cells being treated with **BDP@cRGD-RBC**, there was a *ca.* 5-fold increase in cell death upon light irradiation, in which the population of apoptotic cells was significantly higher than that of necrotic cells. For the MCF-7 cells, a low percentage (< 7%) of cell death population was observed both in the absence and presence of light irradiation. These flow cytometric data suggested that apoptosis is a major cell death pathway for this cell-based photosensitiser.

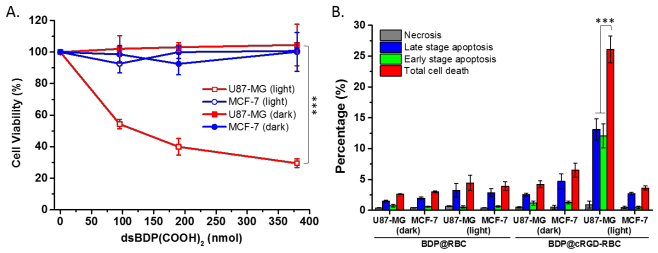

Fig. 7 (A) Cell viability assay for U87-MG and MCF-7 cells after incubation with **BDP@cRGD-RBC** for 30 min in the absence or presence of light irradiation (λ > 610 nm, 23 mW cm^{-2}, 28 J cm^{-2}). Data are expressed as the mean ± SEM of three independent experiments, each performed in quadruplicate. (B) Percentage of necrotic, apoptotic and total cell death of U87-MG and MCF-7 cells after being treated with **BDP@RBC** or **BDP@cRGD-RBC** in the absence or presence of light irradiation (λ > 610 nm, 23 mW cm^{-2}, 28 J cm^{-2}). Data are expressed as the mean ± SEM of three independent experiments. ***p < 0.001 as calculated by the Student's t-test.

Conclusion

In summary, we have developed a facile live-cell surface modification method. By using a bifunctional linker that consists of the bis(bromomethyl)phenyl and OPA moieties, peptide cyclisation and cell-surface conjugation could be performed *in situ* on RBCs. By using this strategy, a cell-based photosensitising system with cyclic RGD moieties on the surface of RBCs loaded with BODIPY-based photosensitiser molecules has been prepared. It exhibits high selectivity against $\alpha_v\beta_3$ integrin-overexpressed cancer cells. Upon light irradiation, it can generate ROS efficiently and release the photosensitiser molecules into the cancer cells, causing substantial photocytotoxicity through predominately an apoptotic pathway.

Author Contributions

W.-P. Fong, C. T. T. Wong and D. K. P. Ng designed the overall studies. C. T. T. Wong, J. C. H. Chu, S. Y. Y. Ha and C. Shao performed the experiments. J. C. H. Chu, C. T. T. Wong and D. K. P. Ng wrote the manuscript.

Conflicts of interest

There are no conflicts to declare.

Acknowledgements

This work was supported by a grant from the Research Grants Council of the Hong Kong Special Administrative Region (Ref. No. 14303320).

References

1 E. Armingol, A. Officer, O. Harismendy and N. E. Lewis, *Nat. Rev. Genet.*, 2021, **22**, 71-88.
2 J. Park, B. Andrade, Y. Seo, M.-J. Kim, S. C. Zimmerman and H. Kong, *Chem. Rev.*, 2018, **118**, 1664-1690.
3 D. Y. Lee, B.-H. Cha, M. Jung, A. S. Kim, D. A. Bull and Y.-W. Won, *J. Biol. Eng.*, 2018, **12**, 28.
4 Q. Wang, H. Cheng, H. Peng, H. Zhou, P. Y. Li and R. Langer, *Adv. Drug Deliv. Rev.*, 2015, **91**, 125-140.
5 X. Bi, J. Yin, A. C. Guanbang and C.-F. Liu, *Chem. Eur. J.*, 2018, **24**, 8042-8050.
6 N. Duszenko, D. M. van Willigen, M. M. Welling, C. M. de Korne, R. van Schuijlenburg, B. M. F. Winkel, F. W. B. van Leeuwen and M. Roestenberg, *ACS Infect. Dis.,* 2020, **6**, 1734-1744.
7 M. T. Stephan and D. J. Irvine, *Nano Today*, 2011, **6**, 309-325.
8 C. M. Csizmar, J. R. Petersburg and C. R. Wagner, *Cell. Chem. Biol.,* 2018, **25**, 931-940.
9 S. Tan, T. Wu, D. Zhang and Z. Zhang, *Theranostics,* 2015, **5**, 863-881.
10 P. Shi, X. Wang, B. Davis, J. Coyne, C. Dong, J. Reynolds and Y. Wang, *Angew. Chem. Int. Ed.,* 2020, **59**, 11892-11897.
11 A. Lamoot, A. Uvyn, S. Kasmi and B. G. De Geest, *Angew. Chem. Int. Ed.,* 2021, **60**, 6320-6325.
12 P. Shi and Y. Wang, *Angew. Chem. Int. Ed.*, 2021, **60**, 11580-11591.
13 H. Lee, N. Kim, H. B. Rheem, B. J. Kim, J. H. Park and I. S. Choi, *Adv. Healthcare Mater.*, 2021, **10**, 2100347.
14 C. L. Tung, C. T. T. Wong, E. Y. M. Fung and X. Li, *Org. Lett.,* 2016, **18**, 2600-2603.
15 Y. Zhang, Q. Zhang, C. T. T. Wong and X. Li, *J. Am. Chem. Soc.,* 2019, **141**, 12274-12279.
16 C. T. T. Wong, J. C. H. Chu, S. Y. Y. Ha, R. C. H. Wong, G. Dai, T.-T. Kwong, C.-H. Wong and D. K. P. Ng, *Org. Lett.,* 2020, **22**, 7098-7102.
17 D. E. J. G. J. Dolmans, D. Fukumura and R. K. Jain, *Nat. Rev. Cancer*, 2003, **3**, 380-387.
18 D. van Straten, V. Mashayekhi, H. de Bruijn, S. Oliveira and D. Robinson, *Cancers*, 2017, **9**, 19.
19 M. Lan, S. Zhao, W. Liu, C.-S. Lee, W. Zhang and P. Wang, *Adv. Healthcare Mater.*, 2019, **8**, 1900132.

20 S. Monro, K. L. Colón, H. Yin, J. Roque III, P. Konda, S. Gujar, R. P. Thummel, L. Lilge, C. G. Cameron and S. A. McFarland, *Chem. Rev.*, 2019, **119**, 797-828.
21 P.-C. Lo, M. S. Rodríguez-Morgade, R. K. Pandey, D. K. P. Ng, T. Torres and F. Dumoulin, *Chem. Soc. Rev.,* 2020, **49**, 1041-1056.
22 X. Sun, C. Wang, M. Gao, A. Hu and Z. Liu, *Adv. Funct. Mater.,* 2015, **25**, 2386-2394.
23 W. Tang, Z. Zhen, M. Wang, H. Wang, Y.-J. Chuang, W. Zhang, G. D. Wang, T. Todd, T. Cowger, H. Chen, L. Liu, Z. Li and J. Xie, *Adv. Funct. Mater.,* 2016, **26**, 1757-1768.
24 F. Pierigè, S. Serafini, L. Rossi and M. Magnani, *Adv. Drug Deliv. Rev.*, 2008, **60**, 286-295.
25 J. Yan, J. Yu, C. Wang and Z. Gu, *Small Methods*, 2017, **1**, 1700270.
26 Z. Chen, Q. Hu and Z. Gu, *Acc. Chem. Res.,* 2018, **51**, 668-677.
27 J. C. H. Chu, C. Yang, W.-P. Fong, C. T. T. Wong and D. K. P. Ng, *Chem. Commun.,* 2020, **56**, 11941-11944.
28 J. C. H. Chu, W.-P. Fong, C. T. T. Wong and D. K. P. Ng, *J. Med. Chem.,* 2021, **64**, 2064-2076.
29 J. C. H. Chu, M. L. Chin, C. T. T. Wong, M. Hui, P.-C. Lo and D. K. P. Ng, *Adv. Therap.,* 2021, **4**, 2000204.
30 S. E. Park, M. I. Sajid, K. Parang and R. K. Tiwari, *Mol. Pharm.*, 2019, **16**, 3727-3743.
31 A. Zorzi, K. Deyle and C. Heinis, *Curr. Opin. Chem. Biol.*, 2017, **38**, 24-29.
32 T. Entradas, S. Waldron and M. Volk, *J. Photochem. Photobiol. B*, 2020, **204**, 111787.
33 C. H. Villa, D. B. Cines, D. L. Siegel and V. Muzykantov, *Transfus. Med. Rev.,* 2017, **31**, 26-35.
34 S. Y. Y. Ha, R. C. H. Wong, C. T. T. Wong and D. K. P. Ng, *Eur. J. Med. Chem.*, 2019, **174**, 56-65.
35 L. Galluzzi and I. Vitale, *Cell Death Differ.*, 2018, **25**, 486-541.
36 H. M. Shen, C. Y. Shi, Y. Shen and C. N. Ong, *Free Rad. Biol. Med.*, 1996, **21**, 139.